THE ASTROPHYSICAL JOURNAL, 494:840–850, 1998 February 20

NONLINEAR MAGNETOHYDRODYNAMIC EVOLUTION OF LINE-TIED CORONAL LOOPS

ROBERTO LIONELLO[1] AND MARCO VELLI
Dipartimento di Astronomia e Scienza dello Spazio, Università di Firenze, Largo Fermi 5, I-50125 Firenze, Italy; lionel@arcetri.astro.it, velli@arcetri.astro.it
GIORGIO EINAUDI
Dipartimento di Fisica, Università di Pisa, Piazza Torricelli 2, I-56126 Pisa, Italy; einaudi@astr11pi.difi.unipi.it
AND
ZORAN MIKIĆ
Science Applications International Corporation, 10260 Campus Point Drive MS-C2, San Diego, CA 92121-1578; mikic@iris023.saic.com
Received 1997 March 27; accepted 1997 September 30

ABSTRACT

Simulations of the nonlinear evolution of the $m = 1$ kink mode in magnetic flux tubes with line-tying boundary conditions are presented. The initial structure of the flux tube is intended to model a solar coronal loop that either has evolved quasi-statically through sequences of equilibria with increasing twist due to the application of localized photospheric vortex flows or has emerged with a net current through the photosphere. It is well known that when the twist exceeds a critical value that depends on its radial profile and on the loop length, the loop becomes kink unstable. The nonlinear evolution of the instability is followed using a three-dimensional MHD code in cylindrical geometry, in different types of magnetic field configurations, with the common property that the current is confined within the same radius, so that the magnetic field is potential in the external regions. The differences reside in the net axial current carried by the structure, ranging from a vanishing current (corresponding to an outer axial potential field) to a high current (corresponding to an outer almost azimuthal potential field). It is shown that, during the nonlinear phase of the instability, loops develop current sheets and, consequently, their evolution becomes resistive with the occurrence of magnetic reconnection. The dependence of the topology of the currents at saturation on the initial magnetic structure, the details of the reconnection phenomenon, and the resistive dissipation mechanism are examined. Finally, the impact of the results on the understanding of coronal activity is discussed.

Subject headings: MHD — Sun: corona — Sun: magnetic fields

1. INTRODUCTION

The existence of long-lived magnetic loop structures in the solar corona has driven a great amount of work on the linear stability of axially symmetric equilibria. The reason for the stability of coronal current-carrying loops has been recognized to be the effect of line-tying, i.e., the axial boundary conditions due to the high-density photosphere. For a given radial profile of the current density, there exists a critical length above which the structure is magnetically unstable (Raadu 1972; Hood & Priest 1979, 1981; Einaudi & Van Hoven 1981, 1983; Velli, Einaudi, & Hood 1990a; Foote & Craig 1990).

Axially symmetric force-free equilibria may be divided into two generic classes: equilibria that contain a nonvanishing net axial current and that have a poloidal magnetic field which decreases as $1/r$ at large distances from the loop axis, and equilibria for which the poloidal field vanishes at the edge of the current-carrying region, which therefore carry a zero net axial current. The latter type of equilibrium is obtained when a magnetic structure, which is initially close to potential, is energized by currents induced via the magnetic field footpoint motions. Short correlation-time motions produce a random energy input, while longer correlation-time motions are capable of a quasi-coherent energy input that may be stored in a stable fashion in a coronal loop, provided the loop is not too long (Mikić, Schnack, & Van Hoven 1989, 1990). The typical loop generated in this way carries a net axial current that vanishes beyond a radius comparable in dimension to that of the region of random motions.

The former kind of equilibrium requires a closing current to flow within the photosphere and may arise when a magnetic flux tube emerges from below the photosphere carrying a net axial current; as the emergence proceeds the loop becomes longer, reaching its critical stability length and crossing this threshold.

In reality, the distinction between such cases is probably not a strong one, as loops are continually excited by footpoint motions as well as emerging in a nonpotential manner from the photosphere. Nonetheless, we consider both cases here.

In this paper we study the evolution of a coronal loop when it becomes unstable, adopting different initial configurations that are intended to model its structure at the end of the energy buildup phase, which is not followed in time. Therefore, we start the simulations by perturbing an equilibrium at a chosen "distance" from marginal stability, as we shall discuss in more detail below. Linear instability results are fundamental in determining the thresholds for the onset of dynamical behavior; the ideal linear eigenfunctions may also be used as initial perturbations in a fully nonlinear simulation.

The paper is organized as follows. In § 2 we present the physical model used, the equations solved, and the bound-

[1] Now at Science Applications International Corporation, 10260 Campus Point Drive MS-C2, San Diego, CA 92121-1578.

ary conditions adopted, as well as the basics of the code used to integrate the nonlinear equations. Section 3 is devoted to the equilibrium configurations and linear stability of the line-tied loops, for which nonlinear simulations are presented in § 4. Finally, in § 5 we discuss the application of our results to solar coronal physics.

2. PHYSICAL MODEL

We represent coronal loops as magnetic flux tubes in cylindrical coordinates (r, θ, z), as in Figure 1. Toroidicity of the loop and gravity are neglected because they are second order in the inverse loop aspect ratio; typical coronal loops have a large aspect ratio, of order 10, in the solar corona.

In our model a loop with a length L extends longitudinally from $z = -L/2$ to $z = L/2$, where the magnetic footpoints are embedded in the dense photosphere. At $r = R$ we place an artificial perfectly conducting boundary. Its influence on the evolution of the system is negligible, provided R is distant enough from the region of appreciable current density.

The evolution of the system is governed by the resistive MHD equations that we write in a nondimensional form as

$$\frac{\partial \boldsymbol{A}}{\partial t} = \boldsymbol{v} \times \boldsymbol{B} - \eta \nabla \times \nabla \times \boldsymbol{A} , \tag{1}$$

$$\frac{\partial \rho}{\partial t} = -\nabla \cdot (\rho \boldsymbol{v}) , \tag{2}$$

$$\frac{\partial p}{\partial t} = -\nabla \cdot (p\boldsymbol{v}) - (\gamma - 1) p \nabla \cdot \boldsymbol{v} + (\gamma - 1)\left[\eta J^2 - \rho \boldsymbol{v} \cdot \frac{\nabla \cdot (v\rho_0 \nabla \boldsymbol{v})}{\rho_0}\right], \tag{3}$$

$$\frac{\partial \boldsymbol{v}}{\partial t} = -\boldsymbol{v} \cdot \nabla \boldsymbol{v} + \frac{\boldsymbol{J} \times \boldsymbol{B}}{\rho} - \frac{\nabla p}{\rho} + \frac{\nabla \cdot (v\rho_0 \nabla \boldsymbol{v})}{\rho_0} . \tag{4}$$

As usual, $\boldsymbol{A}$ is the vector potential of the magnetic field $\boldsymbol{B} = \nabla \times \boldsymbol{A}$, $\boldsymbol{J} = \nabla \times \boldsymbol{B}$ is the current density, $\boldsymbol{v}$ is the velocity, p the pressure, ρ the mass density, η the resistivity, and γ is the specific heat ratio (set equal to 5/3). The primary function of the viscosity operator in the momentum equation is to dissipate energy at the grid scale; for simplicity and speed the density ρ_0 is therefore chosen to be the average poloidal density. The resistivity η can be set to zero to study ideal MHD phenomena or to a finite value to investigate resistive MHD instabilities. In the energy equation we have neglected thermal conduction, radiation, and additional sources of heating, given that at present we are not including a realistic treatment of the thermodynamics of the loop boundaries (transition region and chromosphere).

The line-tying boundary conditions are modeled using the following equations:

$$\frac{\partial \boldsymbol{A}}{\partial t} = 0 , \tag{5}$$

$$\boldsymbol{v} = 0 , \tag{6}$$

at $z = \pm L/2$ and $r = R$, which means that we consider the photosphere as a rigid, perfectly conducting wall (Velli et al. 1990a).

We specify three normalization values: for the magnetic field (B_0), length (L_0), and density (ρ_0), to convert physical quantities from nondimensional to cgs units.

Then all the fields in equations (1)–(4) can be evaluated in terms of

$$A_0 \equiv B_0 L_0 \quad (\text{G cm}) ,$$
$$V_0 \equiv B_0 (4\pi\rho_0)^{-1/2} \quad (\text{cm s}^{-1}) ,$$
$$J_0 \equiv cB_0 (4\pi L_0)^{-1} \quad (\text{statamp cm}^{-2}) ,$$
$$P_0 \equiv B_0^2 (4\pi)^{-1} \quad (\text{dyne cm}^{-2}) ,$$
$$t_0 \equiv L_0 B_0^{-1} (4\pi\rho_0)^{1/2} \quad (\text{s}) ,$$
$$\eta_0 \equiv (4\pi)^{1/2} c^{-2} \rho_0^{-1/2} B_0 L_0 \quad (\text{s}) ,$$
$$v_0 \equiv B_0 L_0 (4\pi\rho_0)^{-1/2} \quad (\text{cm}^2\ \text{s}^{-1}) .$$

3. EQUILIBRIUM AND LINEAR STABILITY

We will consider only force-free equilibria because of the fact that coronal plasmas are low-β plasmas. The equi-

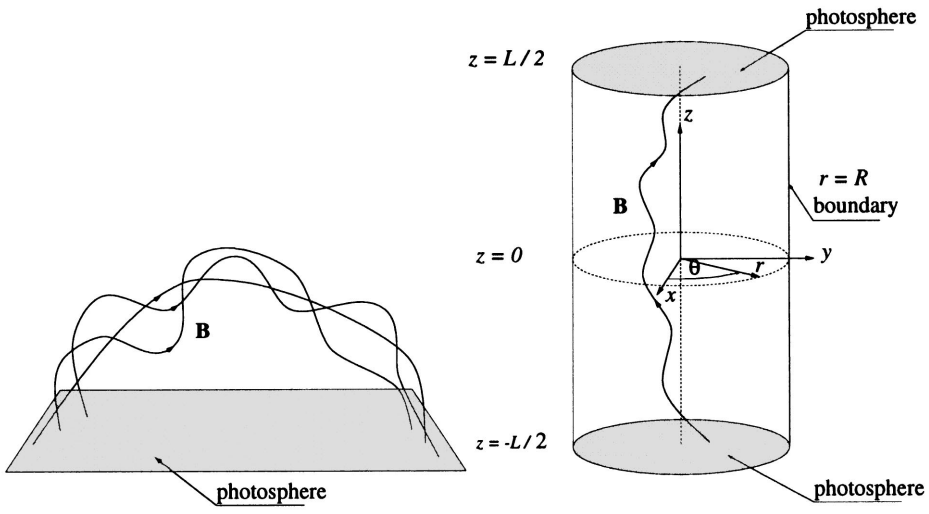

FIG. 1.—Cylindrical coordinate system (r, θ, z) for modeling coronal loops. At $z = \pm L/2$, the photosphere anchors the magnetic footpoints. The "straightened-out" cylindrical loop on the right is intended to model the large aspect ratio coronal loop on the left.

librium equation,

$$\frac{\partial}{\partial r}\left(\frac{B_\theta^2 + B_z^2}{2}\right) + \frac{B_\theta^2}{r} = 0 , \tag{7}$$

does not in itself determine the radial profiles of B_θ and B_z, since one must supply a second equation relating B_θ to B_z. Such a relationship can come from specifying either the radial profile of the twist,

$$\Phi(r) = \frac{LB_\theta}{rB_z} , \tag{8}$$

the ratio between the magnetic field and the parallel current density,

$$\alpha = \frac{\boldsymbol{J}\cdot\boldsymbol{B}}{B^2} , \tag{9}$$

or one component of $\boldsymbol{B}$.

In this paper we concentrate on loop models in which the current is confined within a certain radius, so that the magnetic field is potential in the external regions. In particular, we consider two different classes of field models (hereafter FC and NC; Velli, Lionello, & Einaudi 1997): in the FC class of equilibria, the field has a finite current flowing in the central region of the loop, while in NC class upflowing and downflowing currents yield a null total current in the loop. To derive such models it is convenient to specify the radial profile of α in the case FC and the θ-component of the magnetic field in the case NC. The FC models we will consider belong to a family of equilibria proposed by Chiuderi & Einaudi (1981), which is characterized by

$$\alpha(r) = \begin{cases} \alpha_0 & \text{for } r \le r_0 , \\ \dfrac{\alpha_0}{2}\left[1 + \cos\dfrac{\pi}{\delta}(r - r_0)\right] & \text{for } r_0 < r \le r_0 + \delta , \\ 0 & \text{for } r_0 + \delta < r . \end{cases} \tag{10}$$

The magnetic field scale B_0 is specified once the value of the axial magnetic field component at the origin is assigned, $B_z(0) = 1$. The actual values of B_θ and B_z can be calculated by integrating numerically the equation $\nabla \times \boldsymbol{B} = \alpha\boldsymbol{B}$. In the following we will consider two examples, both presenting a current channel with $r_0 = 0.1$ and $\delta = 4.9$ and therefore a radius of $r = 5$: the first (hereafter referred to as FC1) has $\alpha_0 = 1.0$, whereas the second FC2 has $\alpha_0 = 0.712$ and therefore a smaller amount of twist.

The NC field is a force-free equilibrium that resembles the equilibrium obtained by twisting an initially potential axial magnetic field with a slow and localized photospheric flow (Mikić et al. 1990). In such a model the upflowing and downflowing axial current densities are concentrated inside the radius $r = 5$ and balance in order to yield a null total current. Consequently B_θ differs from zero only for $r < 5$, and the field is purely axial in the potential region. The reason why such an equilibrium models the natural outcome of a localized twist applied at the axial boundary of a potential field is that a localized shearing of magnetic field footpoints generates a poloidal magnetic field component which is restricted in volume to the vicinity of the sheared regions. Ampère's law then guarantees that the net current flowing in the loop remains zero.

We will consider a configuration in which B_θ peaks midway through the current carrying region with the following profile (Lionello 1997):

$$B_\theta = \begin{cases} 0.8\lambda(4 + 2\sqrt{2})r & \text{for } 0 \le r \le 1.25\sqrt{2} , \\ \lambda[-(0.8r - 2)^2 + 2] & \text{for } 1.25\sqrt{2} < r \le 3.75 , \\ \lambda(0.8r - 4)^2 & \text{for } 3.75 < r \le 5 , \\ 0 & \text{for } r > 5 . \end{cases} \tag{11}$$

B_θ and its first derivative are continuous. Hence

$$J_z = \frac{1}{r}\frac{\partial}{\partial r}(rB_\theta)$$

is also continuous and its total flux (current) through any circular axial section, with radius greater or equal than 5, is zero. Using the equation $\boldsymbol{J} \times \boldsymbol{B} = 0$, it is easy to derive the expression for B_z^2 as

$$B_z^2(r) = -B_\theta^2(r) - 2\int_0^r \frac{B_\theta^2}{s}\, ds + C . \tag{12}$$

Again, all quantities are normalized to the length scale L_0 and to the magnetic field scale B_0 in such a way that the value of the axial magnetic field component at the origin is $B_z(0) = 1$. The value of the parameter 2λ, representing the maximum value of B_θ attained at $r = 2.5$, is taken as $\lambda = 0.316$ in order to maximize the twist.

The radial profiles of the magnetic field components along with the relative twist are shown in Figure 2.

We investigate the linear stability properties of these equilibria using the approach and numerical code developed by Velli et al. (1990a). Small perturbations of the form $\tilde{\boldsymbol{\xi}}(r, t) = \tilde{\boldsymbol{\xi}}(r)\exp(\gamma t)$ are considered and $\tilde{\boldsymbol{\xi}}(r)$ is then expanded in a Fourier series, following Einaudi & Van Hoven (1981), in both θ and z. Periodicity in θ allows one to consider the most unstable $m = 1$ mode (m being the poloidal wavenumber) separately, while the line-tying boundary conditions imply that all axial wavenumbers are coupled together. Writing

$$\boldsymbol{\xi} = \mathrm{Re}\sum_n \boldsymbol{\xi}_n(r)\exp\{i[\theta + n\pi(z/L + 1)]\} , \tag{13}$$

multiplying the linearized equations of motion by the phase factor $\exp\{i[\theta + n\pi(z/L + 1)]\}$, and integrating in θ and z, an infinite set of coupled differential equations in the components ξ_n (along the radial direction) is obtained. This system of equations represent an eigenvalue problem for the growth rate γ, whose true value can be obtained truncating equation (13) to a total of five Fourier harmonics centered around the wavenumber k_0, corresponding to the fastest growing kink mode in the absence of line-tying, as discussed in Velli et al. (1990a).

In Figure 3 the growth rate of line-tied kink modes as a function of loop length is shown for the three equilibria introduced above in the zero-β and in the incompressible cases.

Let us now briefly discuss the choice of the three initial configurations whose nonlinear evolution will be discussed in detail in this paper on the basis of their linear stability properties. It is evident from Figure 3 that equilibria NC and FC2 have the same critical length ($L_{\mathrm{crit}} = 36$); for a given length of the loop, the two configurations have a comparable linear phase (i.e. the growth rate of the ideal

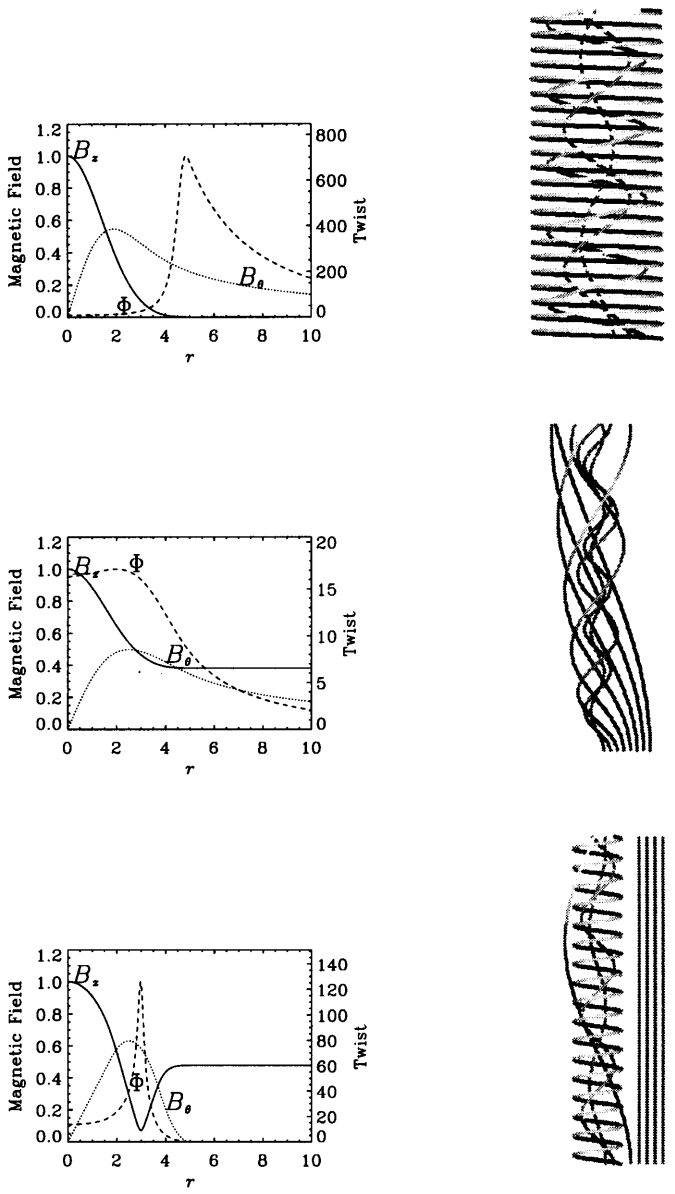

FIG. 2.—Magnetic field components B_z and B_θ and twist Φ (in radians) vs. radius, for equilibria FC1 (*top panel*), FC2 (*middle panel*), and NC (*bottom panel*).

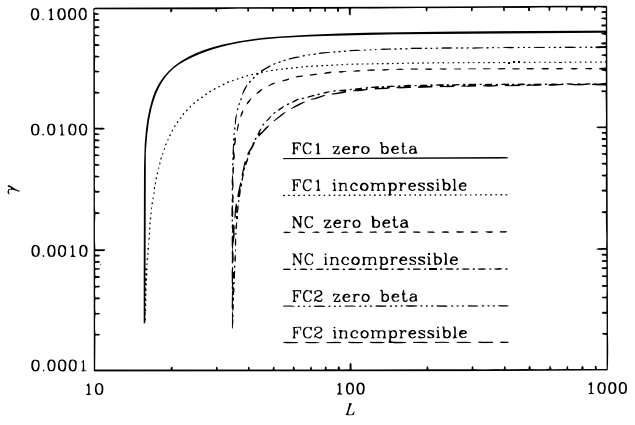

FIG. 3.—Growth rates for the $m = 1$ instability for the three equilibria considered in the presence of line-tying, as functions of the length of the cylinders.

linear instability is about the same for the two equilibria for all possible lengths). Equilibrium FC1 has a shorter critical length, $L_{\rm crit} = 16$, and a given growth rate is achieved in this case for a shorter length of the loop. A fundamental difference exists as far as the linear mode structure for the three equilibria is concerned. From the Fourier components of the radial displacement of the eigenfunction, properly truncated as discussed above, one may obtain its overall r- and z-dependence,

$$\xi(r, \theta, z) = \mathrm{Re}\ \exp\,[i(\theta + k_0 z)] \sum_n \exp\,[in\pi(z/L + 1)]$$
$$= \mathrm{Re}\ \exp\,\{i[\theta + k_0 z + \phi(r, z)]\}\psi(r, z)\,. \quad (14)$$

Surface plots of the function $\psi(r, z)$ are shown in Figure 4 for the three equilibria considered above. In all cases $\psi(r, z)$ has a maximum at the loop apex and decays monotonically to zero at the axial boundary. As far as the radial dependence is concerned, in all cases $\psi(r, z)$ has a maximum well within the current channel and then for FC-type equilibria the radial displacement of the plasma shows a monotonic and slow decay toward zero at the boundary, so that the perturbed current is nonzero even far into the potential equilibrium region. In the case of equilibrium NC on the other hand the radial displacement of the plasma column appears to be confined within a well defined radius. It appears therefore that the FC's fields are subject to the so-called *global* kink mode, whereas the NC field is unstable against the *internal* kink mode.

A further consequence of the ideal mode may be gathered by inspecting the radial component of the perturbed magnetic field. Where this component vanishes, one expects resistive modifications to become important, such as reconnection of magnetic field lines (Velli, Einaudi, & Hood 1990b):

$$B_r(r, \theta, z) = \boldsymbol{B} \cdot \nabla\xi$$
$$= \mathrm{Re}\ \exp\,[i(\theta + k_0 z)] \sum_n \left[\frac{B_\theta}{r} + \left(k_0 + \frac{n\pi}{L}\right)B_z\right]$$
$$\times\ \xi_n(r)\exp\,[in\pi(z/L + 1)]$$
$$= \mathrm{Re}\ \exp\,\{i[\theta + k_0 z + \phi_b(r, z)]\}\psi_b(r, z)\,. \quad (15)$$

The function $\psi_b(r, z)$ is plotted in Figure 5 as a function of r for various values of z, for the three equilibria considered above. It appears that, for equilibrium FC1, the radial profile for all values of z of $\psi_b(r, z)$ shows a monotonic decay toward 0 at the boundary, while for equilibria FC2 and NC, there exists a point $r = r_s$ at the loop apex where $\psi_b(r, 0) = 0$. This point corresponds to a region of very rapid variation of both $\psi(r, z)$ and $\psi_b(r, z)$ for equilibrium NC, whereas such functions are much smoother for equilibrium FC2. Because the perturbed magnetic field ideally vanishes here, resistive effects cannot be neglected. The contemporary presence of strong perturbed currents then implies that in both cases we may expect resistive effects in the nonlinear evolution of the instability, but on faster timescales because of larger gradients for equilibrium NC.

To summarize the important aspects of the linear theory, there exist equilibrium configurations, here exemplified by models NC and FC2, which tend to form regions where current concentrations and therefore magnetic reconnection can occur. The two equilibria differ substantially in the behavior of the radial displacement, which appears to be much more confined within the current channel for equi-

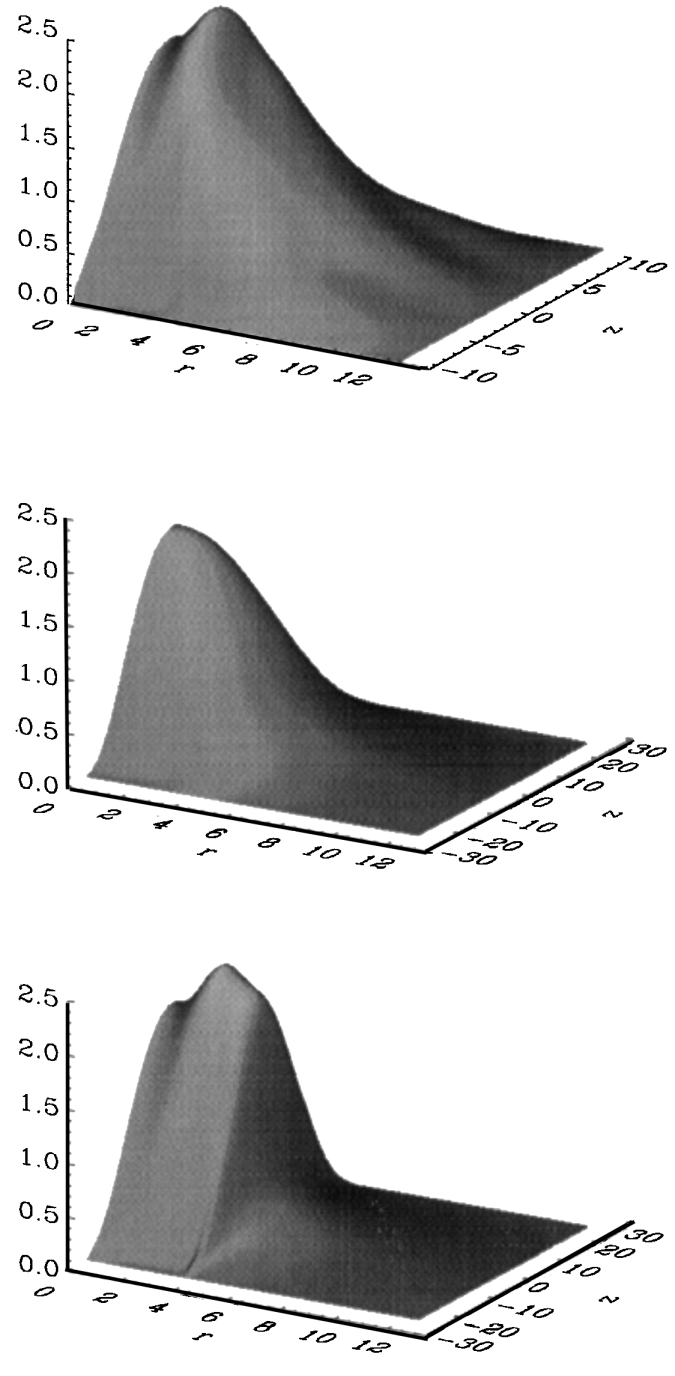

FIG. 4.—Absolute value of the radial linear displacement for equilibria FC1, $L = 20$ (*top panel*); FC2, $L = 50$ (*middle panel*); and NC, $L = 50$ (*bottom panel*).

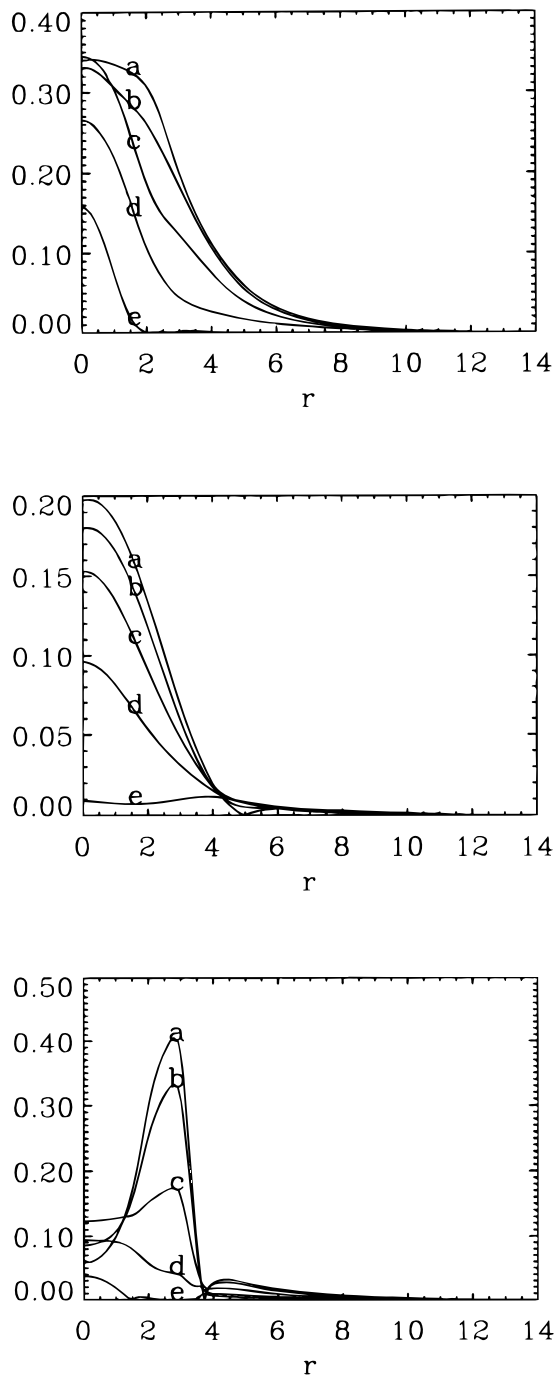

FIG. 5.—Absolute value of the linear radial magnetic field perturbation for equilibria FC1, $L = 20$ (*top panel*); FC2, $L = 50$ (*middle panel*); and NC, $L = 50$ (*bottom panel*). The curves are (*a*) $z = 0$, (*b*) $z = L/8$, (*c*) $z = L/4$, (*d*) $z = 3L/8$, and (*e*) $z = L/2$.

librium NC. This is in contrast with other configurations, such as model FC1, where the plasma displacement is smooth and the radial perturbed magnetic field never vanishes. This result is independent of the length of the structure, once it becomes sufficiently long to be kink unstable.

On the other hand there exist equilibria with a radial structure, such as FC1, that are unstable for lengths considerably smaller than other equilibria with different radial structure, as FC2 and NC. We expect the line-tying boundary conditions to affect the nonlinear evolution more substantially for shorter configurations.

To investigate the differences in the nonlinear evolution due both to the length of the unstable loop and to the presence of "resonant" regions due to the vanishing of the radial perturbed magnetic field, we have chosen to follow such evolution in three cases, namely equilibrium FC1 with $L = 20$, FC2 with $L = 50$, and NC with $L = 50$. The three equilibria are close to but not exactly at marginality in order to speed up the linear phase of the instability and reduce the computing time. In reality the loop becomes unstable either because its twist is raised at a fixed length or because the length grows at fixed twist. In all cases the departure from equilibrium occurs at marginality, but, for the equilibrium we have examined, very little difference in the nonlinear behavior is introduced by our choice because

of the very rapid increase of growth rate as marginality is crossed.

4. NONLINEAR RESULTS

We have performed three simulations to study the nonlinear evolution of kink instabilities that develop in the FC and NC fields. The MHD equations (1)–(4) are advanced numerically in time by means of a three-dimensional semi-implicit algorithm, which makes use of a Fourier expansion in the poloidal direction and of a finite-difference technique in the axial and radial directions. We define a radial mesh extending between $r = 0$ and $r = R$, where we set a conducting boundary. Since we expect to find current concentrations in the vicinity of the center of the cylinder, the mesh is designed as in Mikić et al. (1990), with greater resolution for small r's and increasingly sparser at greater radii: 13% of the points are within $r = 0.05R$, 26% are within $r = 0.1R$, 55% are within $r = 0.25R$, and 82% are within $r = 0.5R$. The ratio of the largest Δr to the smallest is 13.9. R must be large enough to avoid artificial stabilizing effects on the evolution of the system. We choose $R = 20$ for the FC fields, which develop global kink modes, and $R = 12.5$ for the NC equilibrium, in which the internal kink mode is effectively confined by the outer constant axial field. The axial and poloidal meshes are taken to be uniform in both cases. A $63 \times 63 \times 32 r - z - \theta$ mesh is employed. We use a dealiased Fast Fourier Transform algorithm, so that only modes with $0 \leq m \leq 10$ are retained (equivalent to $\frac{2}{3}$ of available Fourier space). The inversion of self-adjoint matrices, generated by the semi-implicit formulation and by the fully implicit treatment of the viscous and resistive terms, is accomplished through a conjugate gradient solver with diagonal preconditioning. The details of the code are described elsewhere (Lionello, Mikić, & Schnack 1998). The initial conditions assume constant mass density, $\rho = 1$, constant temperature, a plasma beta $\beta = 0.01$, which is typical of the solar corona and an $m = 1$ perturbation of amplitude $v \sim 6 \times 10^{-4}$ is applied to the three equilibria described above. In order to save computing time the radial and axial profiles of the initial perturbation are derived from the linear code.

The computation is started with no resistivity and with a small value of the viscosity, $\nu \sim 10^{-3}$, to be able to follow the entire ideal linear phase of the instability. We find that in all three cases during the first stage of the nonlinear ideal evolution small scales are created in all three directions and eventually resistivity *must* be introduced in the computation in order to dissipate the energy which accumulates at small scales and to avoid the development of numerical instabilities (Einaudi et al. 1997). Therefore after a time T_r, whose value depends on the equilibrium under investigation, the resistive terms are turned on with $\eta = 10^{-2}$ ($T_r = 195$, 160, and 115, respectively, for FC1, FC2, and NC), and at the same time the viscosity is set to the same value. Such a value is necessary to describe the behavior of small scales in our moderate resolution simulations properly. Resistivity is actually important only locally where small scales are created by the nonlinear dynamics. Attempts to link the inclusion of resistivity to the magnitude of the currents (to avoid the diffusion of the large-scale structures) in our code were unsuccessful, probably because of the implicit treatment of the dissipative terms.

Once resistivity is turned on, the instability eventually saturates in a timescale that appears to be independent of the equilibrium adopted even though the linear timescales are different. Such a behavior is well described by the time history of the magnetic and kinetic energies contained in the different poloidal modes, which is shown in Figure 6 (note the cusps in the profiles at the time when resistivity is turned on).

In all runs an $m = 0$ transient mode shows up in the kinetic energy history, which is due to adaptation of the analytical equilibria to the grid. We have derived the approximate growth rate of the $m = 1$ mode in the three cases, finding a satisfactory agreement with the growth rates obtained using the linear code presented in Figure 3. From Figure 6 it is also clear that the growth of the higher m modes is due to forcing from the $m = 1$ mode via quadratic nonlinear terms, since, e.g., the $m = 2$ mode, once the $m = 1$ mode is well into the exponential growth phase, also exhibits exponential growth with a rate that is twice as large as that of the $m = 1$.

In order to investigate the distribution of the currents in the loop and to better understand the physical meaning of the creation of small scales, we have computed the modulus of the current density at different heights for the three equilibria at the beginning of the resistive phase, and we present the results for $z = 0$ and $z = \frac{2}{3}L$ in Figure 7. It is evident that the introduction of the resistivity is necessary to correctly describe the evolution of current peaks that have been formed during the ideal nonlinear evolution. The overall topology of the current structure differs considerably from one equilibrium to the other, reflecting the different physical nature of the current concentration. We have already described how for model FC1 the kink extends far into the regions of the original potential field and the current distribution does not show any strong concentration in the linear phase. In the nonlinear phase two current peaks develop, one per each half loop, the location of the peaks depending on the total length of the loop. This fact can be seen comparing the results for FC1 with the results presented in Velli et al. (1996) for their model *a*, which has the same radial structure as FC1 and length $L = 25$. The current concentrations at $z = 0$ are just the "tips" of the two layers developed in the legs of the loop. The formation of such current layers is a direct consequence of the fact that the magnetic lines cannot move at photospheric levels producing strong gradients where the kink folds on itself in each leg of the loop.

The presence of "resonant" regions in the linear phase can be another possible cause for the formation of current concentrations in the subsequent nonlinear phase. In a "resonant" region the ideal terms determining the time evolution of the radial component of the perturbed magnetic field go through zero, generating a current concentration within the region. For both FC2 and NC models the "resonant" region is located at the loop apex and current sheets develop there. The difference between the two models is that in the NC case only the internal part of the plasma column moves outward, piling up magnetic energy at the border with the potential region and contributing to the local enhancement of the current. In the FC2 case the radial displacement is more extended and therefore the resonant region is carried by the flows outward with a smaller opposition of the potential field.

In all cases current layers are formed and the evolution becomes resistive with a consequent occurrence of magnetic reconnection (see also Baty & Heyvaerts 1996).

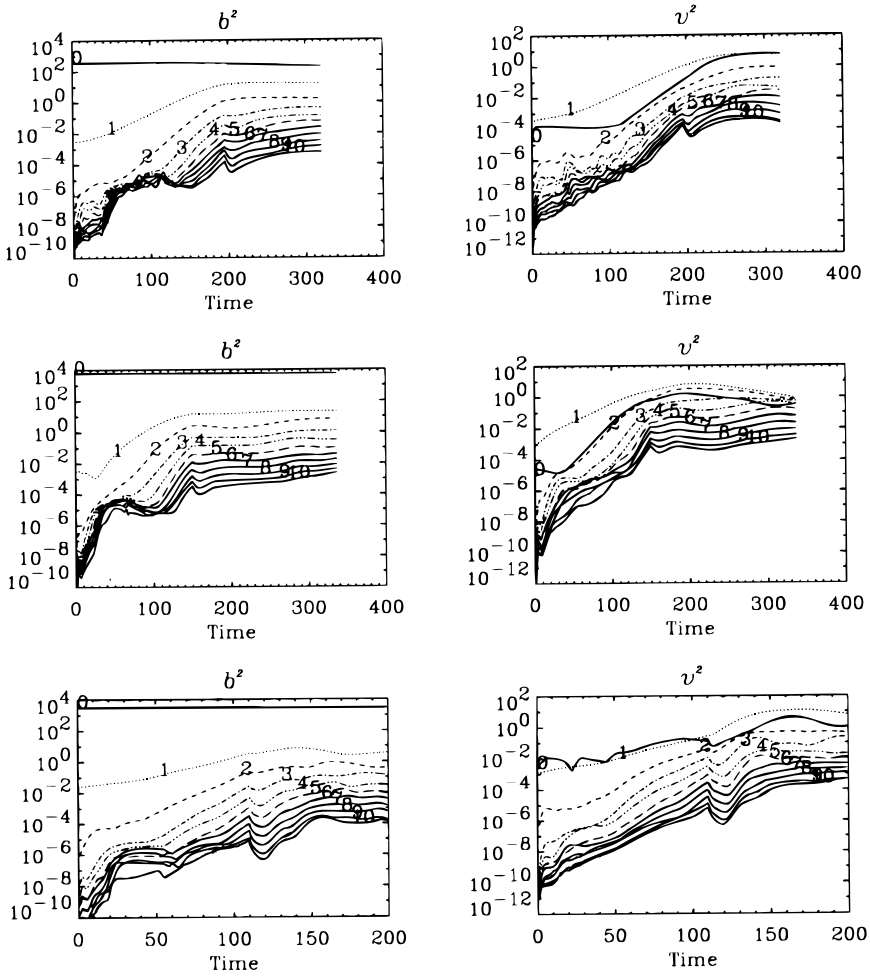

FIG. 6.—Poloidal mode histories of the magnetic and kinetic energy for equilibria FC1 (*top panel*), FC2 (*middle panel*), and NC (*bottom panel*)

In Figures 8 and 9 we present field line plots for the FC and NC models at the beginning of the resistive phase and at saturation of the instability when all poloidal modes start declining. The lines start from the bottom of the loop at different radii ($r = 2, 4$) and angles, in the region where the current flows, and are integrated until they reach the top. This choice of field line imaging makes the representation asymmetrical, though clearly a perfectly symmetrical image would appear if we plotted also the corresponding field lines originating from the top of the loop. The axial dimensions of the structures are proportional to the real lengths of the loops. Each magnetic line connects two fluid elements that are rooted in the photosphere at opposite sides of the loop. During the ideal phase the field line can only be bent and twisted since the fluid elements in the photosphere cannot move. In the resistive phase the field lines can reconnect, altering the field topology and therefore the connectivity between fluid elements in the photosphere.

The fact that reconnection has occurred during the resistive nonlinear evolution of all three models is evident from a comparison of left and right panels in Figures 8 and 9. Following the previous discussion on the properties of the dynamics of the three models, it is not surprising to notice that the final magnetic topologies of the three models differ considerably even if the physical mechanism determining the evolution is the same in all cases. This is due to the fact that the current layers resulting from the ideal nonlinear evolution are located in different regions of the loop. Reconnection starts influencing those magnetic lines that go through the current layer and therefore changes the connectivity of those fluid elements at the photosphere where such lines originate. Away from the current layer the lines are frozen and move with the local velocity of the fluid.

In the case of model FC1 magnetic lines are affected by reconnection in both legs of the loop and the kink progressively involves field lines at greater and greater distances from the axis of the loop. As a result lines with an originally small amount of twist are connected with lines originally in the potential region of the loop with a much greater twist and eventually the original magnetic field topology is completely destroyed, leading to what appears to be an ergodic field. We have not checked whether there are field lines that are actually space filling, or field lines that are totally disconnected from the photosphere, but an indication may be given by the behavior of the function $\alpha = \boldsymbol{j} \cdot \boldsymbol{B}/B^2$, which is a constant along field lines. Initially, this quantity is nonvanishing only within the current channel and monotonically decreasing outward (it does not depend on z). At saturation, this function appears to develop a plateau over the full extent of the perturbed region. At the same time, the field lines are clearly not the laminar constant α force-free field.

Models FC2 and NC develop a current layer at the loop apex and suffer a less extended kink instability. In the NC case the kink is totally confined within the current channel and the original potential field contains no twist. For model

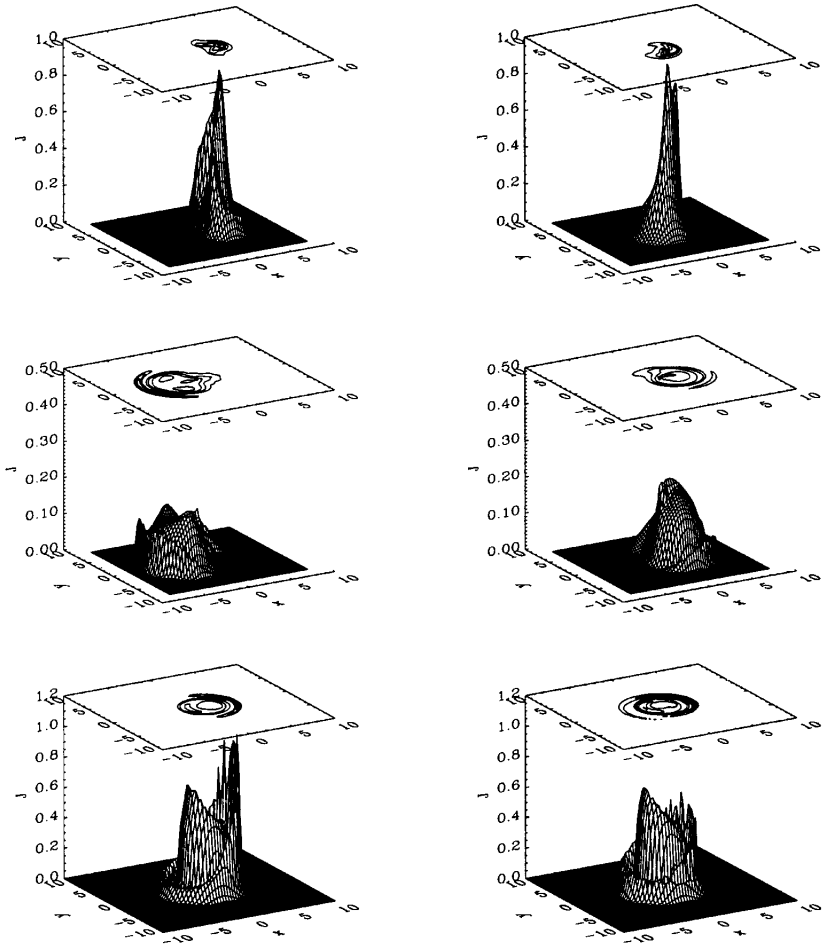

FIG. 7.—Modulus of current density at $z = 0, 2/3L$ in the early resistive phase for equilibria FC1 (*top panel*), FC2 (*middle panel*), and NC (*bottom panel*)

FC2 the kink is slightly more extended and the potential outer field has a nonvanishing twist, but the result is in both cases an unwinding of the inner field lines. While the NC kink is totally confined, the FC2 kink presents a global outward displacement of magnetic surfaces.

A straightforward way of recognizing magnetic reconnection is through the field-line connectivity. In the line-tied case, the presence of static fluid elements at the boundaries simplifies the task of searching for changed connectivity, since all that is required is to find a field line that in moving from the bottom to the top of the loop no longer reaches the same location (radius and/or angle). In Figure 10 we show in the left panel projections of field lines on the (r, θ) plane, for the three runs at the beginning of the resistive phase. We selected two field lines for each run, one which has reconnected (dashed) and one which has not (continuous). The boxes indicate the position at $t = 0$ of the field line footpoint at $z = L/2$, and crosses indicate the field line footpoint at $z = -L/2$. The bars correspond to the position of the field line footpoint at $z = L/2$ in the early resistive phase. When a bar and a box do not coincide the corresponding field line has reconnected somewhere along the loop. The same field lines are plotted in the right panel at a time in the early resistive phase, and the line that reconnects is indicated by an arrow. It is interesting to notice that lines originating at the same radius and different angles may or may not reconnect depending whether they go through the current layer or not. Lines originating at different radii exhibit a similar behavior.

Reconnection proceeds on a timescale that is given by the local nonlinear time, i.e., in such a way as to furnish a sink for the cascade of magnetic energy, of which the current layer represents the preferred dissipative structure. The value of the resistivity we must introduce, is such that the local Reynolds number is of order unity. In other words the current layers start to disrupt when thickness is of the order of the grid size of the simulation. At that point we are constrained to turn on the resistivity and the reconnection process takes place.

During the ideal phase the mechanical energy present in the loop is conserved and the instability produces a transfer of magnetic energy into kinetic energy. At the beginning of the resistive phase the magnetic energy starts to be dissipated. In order to show the efficiency in dissipating magnetic energy of the three models in the resistive phase we present in Figure 11 the time histories of the kinetic and the nonpotential magnetic energies. This is defined as the total magnetic energy less the energy of the underlying axial potential magnetic field, since this is the maximum available energy for dissipation in the structure.

For simplicity we have taken the axial potential field to be the average B_z at $t = 0$, any difference from the true potential field is appreciable only in small layers near the axial boundaries and the energy does not change substantially.

The kinetic energies have a maximum when the saturation of the instability occurs and in all cases the total kinetic energy is much smaller than the total magnetic energy in the

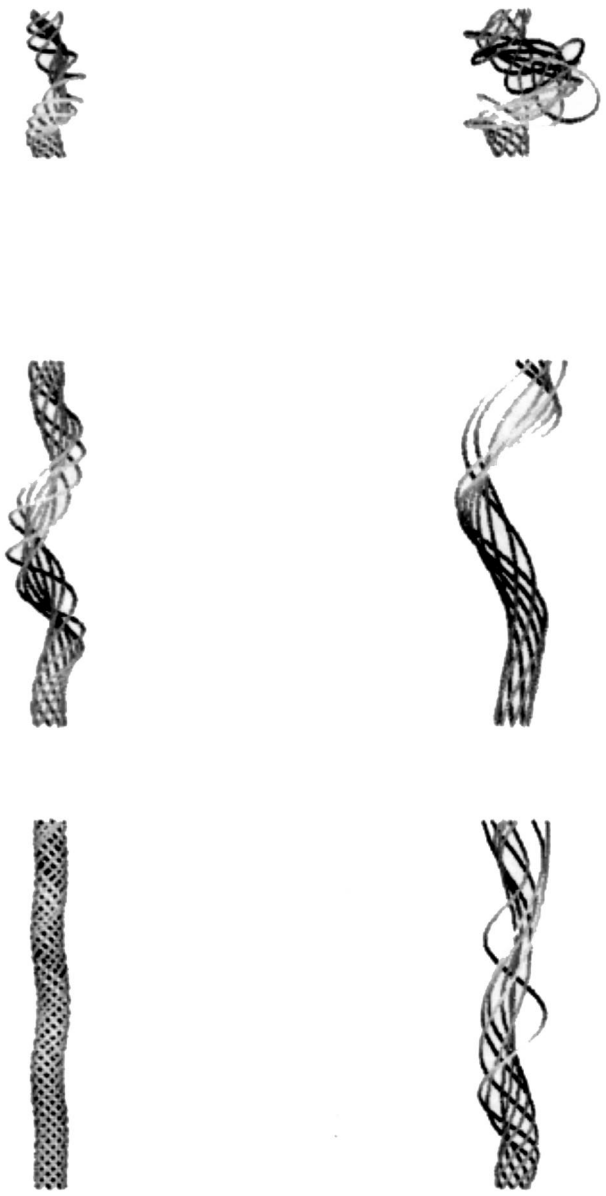

FIG. 8.—Field line plots of field lines with footpoints starting at $r = 2$, $z = -L/2$ in the early resistive phase (*left panel*) and at saturation (*right panel*) for equilibria FC1 (*top panel*), FC2 (*middle panel*), and NC (*bottom panel*).

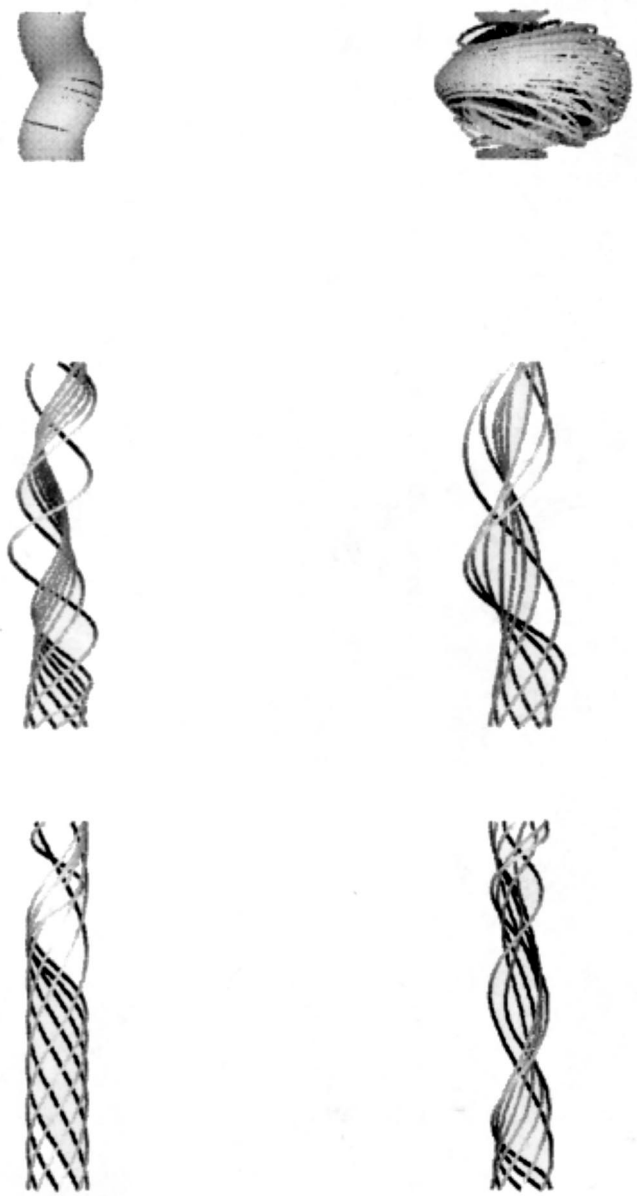

FIG. 9.—Field line plots of field lines with footpoints starting at $r = 4$, $z = -L/2$ in the early resistive phase (*left panel*) and at saturation (*right panel*) for equilibria FC1 (*top panel*), FC2 (*middle panel*), and NC (*bottom panel*).

structure. However, close to the current sheet a local enhancement of the velocity is observed and the vorticity shows the elongated quadrupolar structure with maxima at current sheet edges, typical of the reconnection phenomenon (Velli et al. 1996). There are big differences in the efficiency of the dissipation of the magnetic energy in the three cases. Such differences are due to the different importance of the current layer with respect to the bulk current. In the limit of very small resistivity and viscosity, i.e. in much higher resolution simulations, we expect that all the energy would be dissipated within the current layers that in this case would collapse into genuine sheets.

5. CONCLUSION

We have studied the nonlinear evolution of three magnetic field equilibrium configurations representing models of coronal loops of different origin. In all cases, dynamical evolution is triggered by an ideal kink instability that arises when either the length of the loop or the amount of magnetic twist exceeds a threshold. The simulations were started with a loop twist that is beyond the instability threshold (in the unstable region), with a twist chosen to give comparable growth rates for the three models during the linear phase. The timescale of the instability is on the order of the longitudinal Alfvén time. Our results indicate that the subsequent evolution is not affected strongly by the duration of the linear phase, i.e., how close the initial equilibrium is to marginal stability.

The evolution can be divided into three distinct phases. The first is the ideal, linear phase, whose properties depend strongly on the kind of equilibrium examined. Model FC1 is subject to a global kink mode without the appearance of a "resonant" surface. In contrast, the other two models contain a region at the loop apex where the ideal contribution to the radial component of the induction equation van-

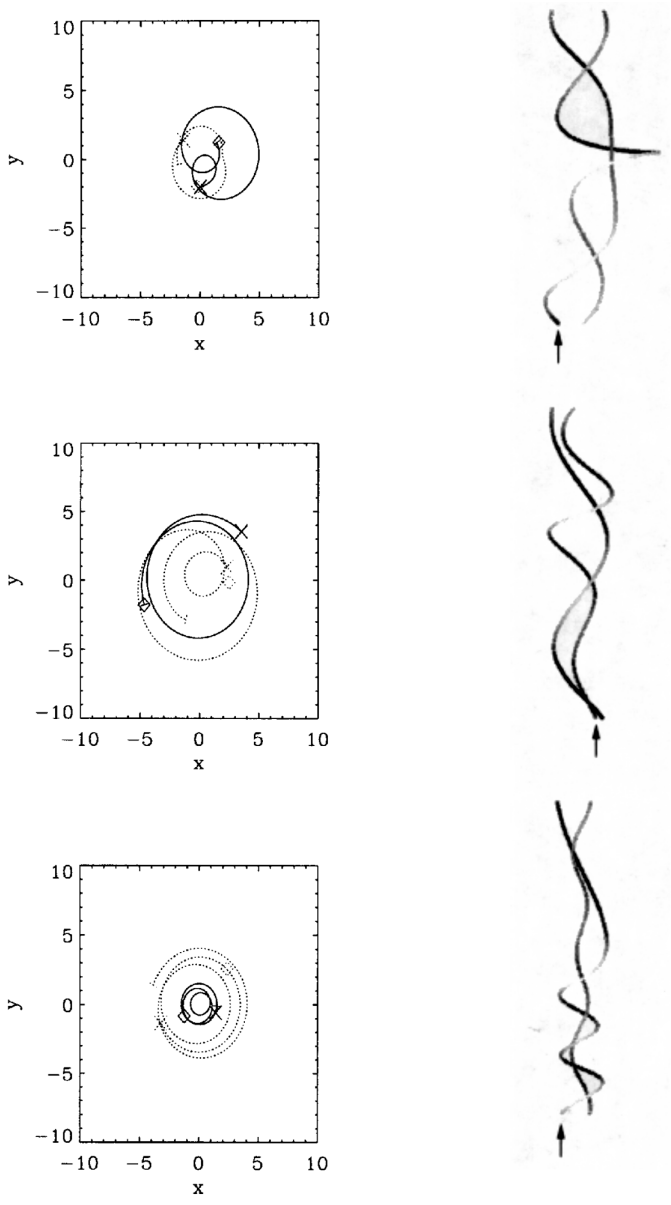

FIG. 10.—Projection on the (r, θ) plane (*left panel*) and three-dimensional plots (*right panel*) of two field lines for equilibria FC1 (*top panel*), FC2 (*middle panel*), and NC (*bottom panel*).

ishes; in this region resistive modifications (i.e., reconnection) can be important. Such "quasi-resonances" in the linear eigenfunction signal locations where the current density tends to concentrate during the nonlinear evolution of the instability. In the case of equilibrium FC2, the radial displacement corresponds to a global kink and the quasi-resonant region is therefore displaced toward the outer potential field region in the subsequent nonlinear ideal phase. For the NC equilibrium, on the other hand, the dominant instability is an "internal" kink mode that is confined by the strong axial potential field: the linear, radial displacement is confined within the quasi-resonant radius and all the dynamics occurs within the current channel.

Once the mode amplitude has grown sufficiently, nonlinear effects become important. During this second phase, the line-tied axial boundary conditions can cause current concentrations to form: magnetic field lines are constrained to fold on themselves somewhere along the legs of the loop, since the displacement is required to vanish at the photospheric footpoints. In contrast, with periodic axial boundary conditions, the kink is allowed to redistribute the magnetic stress in the axial direction. This effect is manifested most clearly in cases with an extended global mode, such as FC1. Our simulations show the formation of current concentrations for all three equilibria. The transverse dimension of the concentrations is of the order of the grid spacing. We have checked that, within the limited spatial resolution accessible to our concentrations a local reduction of the grid size leads to smaller transverse dimensions of the sheet. It is for this reason we dub the resulting current layers "current sheets." The timescale for the formation of the current sheet depends on the growth rate of the ideal instability, and, when the sheet forms as a result of line tying (as in case FC1), also on the loop length. Once the current sheet thickness begins to approach the grid spacing it is necessary to use finite resistivity to correctly follow the subsequent evolution of the configuration.

The principal feature of the resistive evolution is magnetic field line reconnection in the vicinity of the current sheet, with a corresponding change in the topology and connectivity of the magnetic field lines. This characterizes the final relaxation phase. Although the efficiency of the dissipation of magnetic field energy varies among the three models considered, they all share a common feature: an ideal large-scale magnetic instability nonlinearly leads to the formation of current sheets, initiating a cascade of energy to the dissipation scale, where it is dissipated readily. The limited dynamic range in the length scales in our model, imposed by computational constraints of our numerical solution, does not permit us to determine the scaling of the energy release rate to the small values of resistivity appropriate to the solar corona. (Recall that our numerical model requires us to use a plasma resistivity that is many orders of magnitude larger than the value expected in the solar corona.) We are therefore unable to make a *quantitative* estimate of the timescale for energy release in the solar corona. Nevertheless, we expect that the *relative* energy release rates to be meaningful in our model.

The liberation of magnetic energy in the NC model, in which $\frac{2}{3}$ of the initial free magnetic energy is dissipated, is much greater than in the FC models. The NC field also has a more rapid rate of dissipation of magnetic energy. The resistive evolution leads to an unwinding of the magnetic field lines, leaving a configuration that is closer to a potential configuration than the original one. In the NC model, the strong external axial potential field confines the current channel, and contributes to the formation of a strong current sheet. In contrast, when the external potential field is twisted, the current sheet due to the "resonance" is weaker and only a small amount of magnetic energy is dissipated, as exemplified by model FC2.

Our calculations show that the current sheets caused by the line-tying effect depend strongly on the length of the loop: short loops tend to develop stronger current sheets. For example, in model FC1 (which is shorter than loop FC2 by $\frac{2}{5}$), the current sheet (which is localized near the legs of the loop) is stronger than in case FC2, and consequently the amount of magnetic energy dissipated exceeds that in the FC2 case. Since a substantial fraction of the magnetic energy is released, we expect that loops subject to kink instabilities will produce a detectable level of activity. In

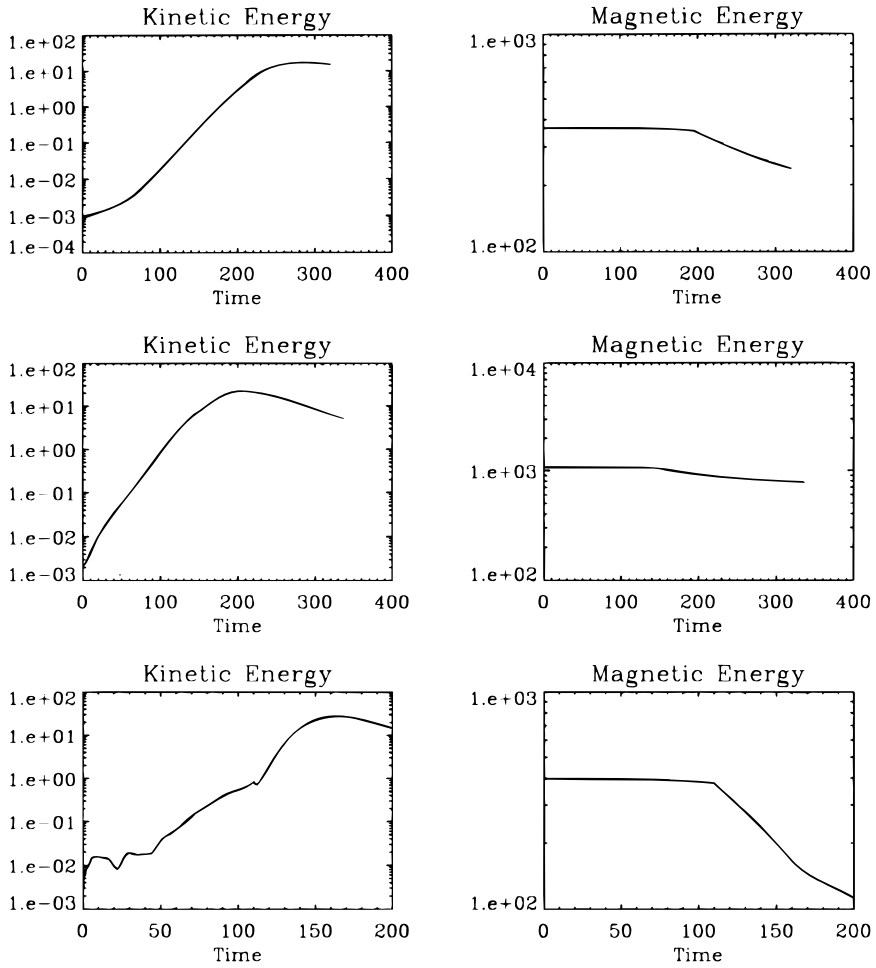

FIG. 11.—Kinetic (*left panel*) and nonpotential magnetic (*right panel*) energies as functions of time for equilibria FC1 (*top panel*), FC2 (*middle panel*), and NC (*bottom panel*).

particular, evolution of equilibrium NC, which maintains its large-scale magnetic structure and evolves on the fastest timescale, may provide a viable physical model for compact loop flares. FC models, which produce weaker current sheets and dissipate smaller amounts of energy, and evolve on longer timescales, would be expected to contribute to coronal heating, and may explain the long-lived hot loops observed by *Yohkoh*.

In summary, line tying has two contrasting effects on the behavior of coronal loops. For sufficiently short loops, it acts as a stabilizing agent to prevent perturbations from growing, allowing loops to build up and store magnetic energy. Once the loops become unstable, line tying can cause current sheets to form, resulting in an enhanced level of energy dissipation compared to non–line-tied configurations. It would be worthwhile to extend the calculations presented here to include a more realistic description of the thermodynamics, and to include the effect of toroidal curvature, which may cause a rapid outward expansion of loops as they are twisted (Amari et al. 1996).

We would like to thank Hubert Baty, Claudio Chiuderi, Jon Linker, Dalton Schnack, and Gerard Van Hoven for helpful discussions. Computations were performed at the Interuniversity Consortium of the Northeastern Italy for Automatic Computing (CINECA) and at the National Energy Research Supercomputer Center (NERSC) at Livermore, California. This work was supported in part by a NASA Space Physics Theory Program contract (NAS 5-96081) to Science Applications International Corporation (SAIC). R. L. wishes to thank Roberto Casini for collaboration in developing imaging software; G. E. and R. L. wish to thank the University of California, Irvine (UCI), and SAIC for their kind hospitality during the development of this work. The visits of G. E. and R. L. to UCI were supported, in part, by NSF and NASA.

REFERENCES

Amari, T., Luciani, J. F., Aly, J. J., & Tagger, M. 1996, ApJ, 466, L39
Baty, H., & Heyvaerts, J. 1996, A&A, 308, 93
Chiuderi, C., & Einaudi, G. 1981, Sol. Phys., 73, 89
Foote, B. J., & Craig, I. J. D. 1990, ApJ, 350, 437
Einaudi, G., Lionello, R., & Velli, M. 1997, Adv. Space Res, 19, 1875
Einaudi, G., & Van Hoven, G. 1981, Phys. Fluids. 24, 1092
———. 1983, Sol. Phys., 88, 163
Hood, A. W., & Priest, E. R. 1979, Sol. Phys., 64, 303
———. 1981, Geophys. Astrophys. Fluid. Dyn., 17, 297
Lionello, R. 1997, Ph.D. thesis, Univ. Florence
Lionello, R., Mikić, Z., & Schnack, D. D. 1998, J. Comput. Phys., in press
Mikić, Z., Schnack, D. D., & Van Hoven, G. 1989, ApJ,338, 1148
———. 1990, ApJ, 361, 690
Raadu, M. A. 1972, Sol. Phys., 22, 425
Velli, M., Einaudi, G., & Hood, A. W. 1990a, ApJ, 350, 419
———. 1990b, ApJ, 350, 428
Velli, M., Lionello, R., & Einaudi, G. 1997, Sol. Phys., 172, 257